#### **PROCEEDINGS A**

royalsocietypublishing.org/journal/rspa



# Research





**Cite this article:** Kraitzman N, Hardenbrook R, Dinh H, Murphy NB, Cherkaev E, Zhu J, Golden KM. 2024 Homogenization for convectionenhanced thermal transport in sea ice. *Proc. R. Soc. A* **480**: 20230747.

https://doi.org/10.1098/rspa.2023.0747

Received: 7 October 2023 Accepted: 28 June 2024

#### **Subject Category:**

Mathematics

#### **Subject Areas:**

applied mathematics, mathematical modelling, climatology

#### **Keywords:**

thermal conductivity, sea ice, advection diffusion processes, convective fluid flow, Stieltjes integrals, Padé approximants

#### **Author for correspondence:**

Noa Kraitzman

e-mail: noa.kraitzman@mg.edu.au

# Homogenization for convection-enhanced thermal transport in sea ice

Noa Kraitzman<sup>1</sup>, Rebecca Hardenbrook<sup>2</sup>, Huy Dinh<sup>3</sup>, N. Benjamin Murphy<sup>3</sup>, Elena Cherkaev<sup>3</sup>, Jingyi Zhu<sup>3</sup> and Kenneth M. Golden<sup>3</sup>

NK, 0000-0003-0813-9616; EC, 0000-0002-5682-5453

Sea ice regulates heat exchange between the ocean and atmosphere in Earth's polar regions. The thermal conductivity of sea ice governs this exchange, and is a key parameter in climate modelling. However, it is challenging to measure and predict due to its sensitive dependence on temperature, salinity and brine microstructure. Moreover, as temperature increases, sea ice becomes permeable, and fluid can flow through the porous microstructure. While models for thermal diffusion through sea ice have been obtained, advective contributions to transport not been considered theoretically. Here, we homogenize a multiscale advection-diffusion equation that models thermal transport through porous sea ice when fluid flow is present. We consider two-dimensional models of convective flow and use an integral representation to derive bounds on the thermal conductivity as a function of the Péclet number. These bounds guarantee enhancement in the thermal conductivity due to the added flow. Further, we relate the Péclet number to temperature, making these bounds useful for global climate models. Our analytic approach offers a mathematical theory which can not only improve predictions of atmosphereice-ocean heat exchanges in climate models, but can provide a theoretical framework for a range of problems involving advection-diffusion processes in various fields of application.

© 2024 The Authors. Published by the Royal Society under the terms of the Creative Commons Attribution License http://creativecommons.org/licenses/by/4.0/, which permits unrestricted use, provided the original author and source are credited.

<sup>&</sup>lt;sup>1</sup>School of Mathematical and Physical Sciences, Macquarie University, Sydney, New South Wales, Australia

<sup>&</sup>lt;sup>2</sup>Department of Mathematics, Dartmouth College, Hanover, NH, USA <sup>3</sup>Department of Mathematics, University of Utah, Salt Lake City, UT, USA

royalsocietypublishing.org/journal/rspa Proc. R. Soc. A 480: 20230747

## 1. Introduction

Heat exchange at the ocean-atmosphere interface is a key driving force in Earth's climate system. In the polar regions, sea ice is a thin, dynamic layer that moderates these exchanges, acting as an insulating blanket on the ocean and reflecting incoming solar radiation. As a material, sea ice is a complex, multi-phase composite with three main constituents: solid pure ice, liquid brine inclusions/channels and air bubbles. The properties of sea ice are determined by the intrinsic properties of each phase, how much of each phase is present and how the components are arranged geometrically. Particularly in sea ice, the thermal properties of the constituents vary over a significant range, with the thermal conductivity of pure ice at its freezing point being about 2.2 W (m K)<sup>-1</sup>, the thermal conductivity of liquid brine smaller by about a factor of four, and that of air smaller by a factor of about 100 [1-3]. Moreover, the thermal conductivity of sea ice changes as the volume fraction of each component varies as a function of temperature and salinity. The complexity of sea ice as a composite material with internal fluid motion makes it challenging to predict its thermal conductivity. Nevertheless, this key parameter is critical to modelling sea ice growth [4,5] and even larger scale dynamics and thermodynamics of the ice cover. In turn, the central role of sea ice in large-scale heat transport in the polar regions and the climate system more broadly makes its thermal conductivity a critical parameter in climate and weather modelling [6–10].

An explicit expression for the thermal conductivity of sea ice is particularly difficult to obtain due to its dependence on the microstructure, namely, the volume fraction, size distribution and connectivity of the brine inclusions as well as the air bubbles. In addition, the thermal properties of sea ice can constantly change due to the sensitivity of the microstructure to changes in temperature and salinity, making the task of obtaining an exact expression for the thermal conductivity of sea ice, or even an accurate theoretical model, quite non-trivial.

Over the past several decades, various models have been proposed for predicting the values of the thermal conductivity of sea ice, accounting for these dependencies on temperature and salinity. The thermal conductivity used in many global climate models is represented by one of the two empirical models fitting the data [11], either the model suggested by Maykut and Untersteiner (MU71) [12] or the bubbly brine (BB) model [8]. However, the expected values of the thermal conductivity of sea ice produced by the MU71 model were positively biased compared with *in situ* experimental measurements [9]. As an improvement, Pringle *et al.* [8] suggested the BB model, which provided a better fit when compared with datasets obtained at temperatures colder than the critical temperature for brine percolation and flow [13]. For a fixed salinity, both the MU71 and the BB models yield values that monotonically decrease as temperature increases.

As the temperature rises, however, sea ice becomes more permeable, and liquid brine with high salt concentration can drain from the sea ice into the ocean, giving way to fresher ocean water, perhaps laden with nutrients, to flow into the icy complex [13,14]. Convective flow is present during the natural solidification of seawater and other binary solutions [15,16]. Moreover, it has been suggested that fluid convection can result in an enhancement of thermal conductivity [9]. This enhancement of the thermal conductivity, once percolation has been initiated, is not captured in either the MU71 or BB models.

For some specific types of fluid flows, such as shear flow, estimates in the form of bounds on effective diffusivity (or effective thermal conductivity) have been obtained [17,18]. However, when considering sea ice, simple velocity fields such as shear flow may not be a good representation of the actual flow field. First-year sea ice, as a mushy layer, can support convective flows both internally and on the ocean-mushy layer interface [15]; see figure 1a. The convection along the interface facilitates the drainage of liquid brine, which is then replenished by fresher seawater flowing through the surrounding channels [15,16,20–22]. Wells *et al.* [19] demonstrated that the observed arrangement of fluid channels correlates with an optimization problem where brine flux is maximized, resulting in convective flows, as illustrated in figure 1b. Moreover,

convection within sea ice is characterized by a distinct pattern of broad upward flows countered by narrow, gravity-driven downward flows through channels, which form as brine drains and ice dissolves [23].

In this study, we examine the thermal conductivity of sea ice in the presence of convective fluid flow. Assuming the convective flow within the sea ice to be continuous, which can be mathematically represented by a Fourier series, we focus on BC and cat's eye flows as depicted in figure 1c. These flow models can be used to represent both internal and ocean–sea ice interface flows. While not perfectly capturing the intricacies of actual convective flows in sea ice, our introduction of these flow fields establishes a foundational basis for deriving bounds and estimates for more realistic continuous flow patterns.

Homogenization techniques offer sophisticated means to encapsulate the complex interplay of physical and thermal properties within a heterogeneous material, such as sea ice, into an *effective* or *bulk* coefficient, transcending the rapidly varying microstructure. This notion of an *effective* property has been used in the study of sea ice thermal behaviour; the expressions for the thermal conductivity and the specific heat derived in [8] and [2,24], respectively, consider effective properties of sea ice that depend only on temperature and salinity. Homogenization methods, such as the analytic continuation method [25–29] or variational principles [30,31], recover the effective properties of a composite material, given information about the individual phases. In general, homogenization can be applied when the microstructure of a material is considered to be composed of period cells with a small length scale relative to the macrostructural scale of the full domain [27,29,32].

The primary goal of homogenization is to replace a detailed equation on the microscale, whose solution may be computationally expensive or provide no insights into the full system behaviour, with a simplified macroscale equation. Figure 2 depicts the process of homogenization to reduce the complexity in the specific case of sea ice. A three-component composite material model of sea ice is detailed in figure 2a, and uniformed sea ice with properties is presented in figure 2b. In this paper, we consider uniformed sea ice filled with cell periodic fluid moving through the ice, as in figure 2c. To obtain bounds on the effective thermal conductivity  $\kappa^*$  of sea ice in the presence of fluid flow, we segment the sea ice domain  $\Omega$  into discrete period sub-cells, each characterized by uniform thermal properties, averaged temperature, and bulk salinity. Moreover, each sub-cell  $\Omega_0$  supports a cell periodic bulk convective fluid flow, as shown in figure 2c. Through this framework, we establish bounds on  $\kappa^*$ , providing a more comprehensive understanding of the impact of convective flow on the thermal properties of sea ice in a global system.

To obtain such bounds on  $\kappa^*$ , we employ an integral representation of the effective thermal conductivity derived originally in [17] to characterize the large-scale, long-time behaviour. This representation involves the Péclet number  $\mathcal{P}$ , a dimensionless number representing the ratio of advective to diffusive transport, and a positive spectral measure  $\mu$  that captures the characteristics of the flow geometry. Murphy *et al.* [33–35] studied the measure  $\mu$  and derived explicit expressions of its moments in the case of a cell periodic fluid flow, as depicted in figure 2c. In this paper, we obtain bounds on the effective thermal conductivity of sea ice in the presence of fluid flow of the forms (2.13) and (2.14) as a function of the Péclet number. Furthermore, for the special case of sea ice, we derive a new representation of the Péclet number as a function of salinity and temperature, which allows us to rewrite our bounds for the effective thermal conductivity of sea ice as a function of temperature. This study contributes to the ongoing development of mathematical models for thermal and diffusive transport through porous sea ice but with the added complexity of convective fluid flow. While it expands on existing frameworks, we introduce novel bounds for the effective thermal conductivity of sea ice with two-dimensional brine flows.

In §2, we derive bounds on  $\kappa^*$  for both a BC flow (2.16) and (2.17) and a cat's eye flow (2.43) and (2.44) as a function of the Péclet number. In §3, we give a new representation for the Péclet

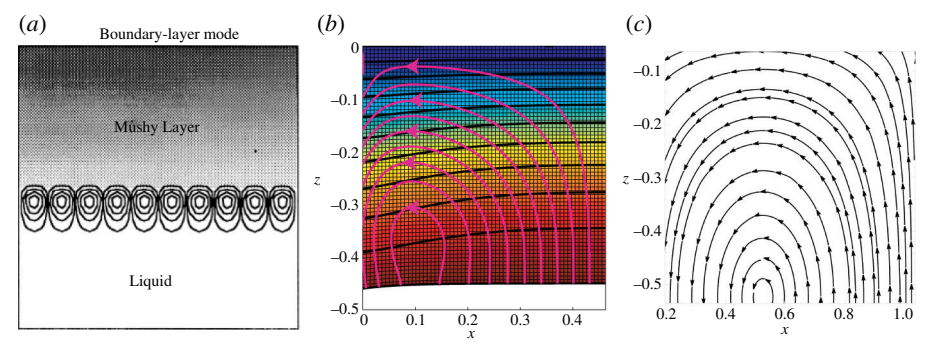


**Figure 1.** (a) Schematics of the convective flow in the ocean—sea ice interface (boundary-layer mode). Reprinted (adapted) with permission from [15]. Copyright 1997, American Chemical Society. (b) Magenta curves represent the streamlines of the convective *bulk* velocity field within sea ice [19]. Reproduced with permission. Copyright 2011, American Geophysical Union. (c) Streamlines for the cat's eye flow of the form  $\mathbf{u} = (-\sin(3x)\cos(3z), \cos(3x)\sin(3z))$ .

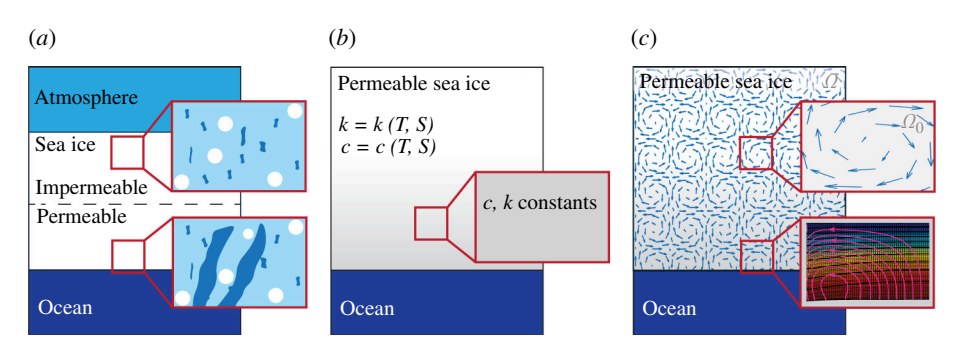


**Figure 2.** Sea ice schematic with ocean below and atmosphere above. (a) The sub-frames show a detailed microstructure with ice, brine inclusions and air bubbles coloured light blue, blue and white, respectively. Permeable sea ice is bounded (dashed line) from above by impermeable sea ice. (b) Uniformed sea ice with properties independent of microstructure. Here thermal properties, such as conductivity  $\kappa$  and specific heat c, depend only on temperature T and salinity S. Locally, thermal properties are taken to be constant (sub-frame). (c) Periodization of the uniformed sea ice domain  $\Omega$  with cell periodic fluid flow  $\mathbf{u} = (-\sin(3x)\cos(3z),\cos(3x)\sin(3z))$ . (Top sub-frame) Sub-cell  $\Omega_0$  has constant thermal properties and periodic flow. (Bottom sub-frame) Streamlines of the convective flow in the interface layer [19]. Panel (c) bottom sub-frame is reproduced with permission. Copyright 2011, American Geophysical Union.

number in terms of temperature and salinity. For fixed salinity, this allows us to obtain bounds on  $\kappa^*$  as a function of temperature; see figure 3. In §4, we quantitatively validate our bounds using Monte–Carlo simulations of a stochastic differential equation (SDE) representing our governing advection–diffusion process; see figure 4a. This is supplemented with a qualitative validation using available in situ measurements of the thermal conductivity of sea ice; see figure 4b. We conclude our results in §5 and discuss the implications of the enhancement of thermal conductivity on the global climate system as well as future work these results motivate.

# 2. Bounds on the effective thermal conductivity of sea ice

In this section, we present the mathematical background and the analytic derivation of the bounds on the effective thermal conductivity of sea ice  $\kappa^*$  in the presence of fluid flow. Let  $\Omega$  be a domain of uniformed sea ice where convective flow is relevant and partitioned into sub-cells. On each sub-cell  $\Omega_0$ , we consider the advection–diffusion equation with constant thermal properties and cell periodic fluid flow. In this framework, homogenization methods

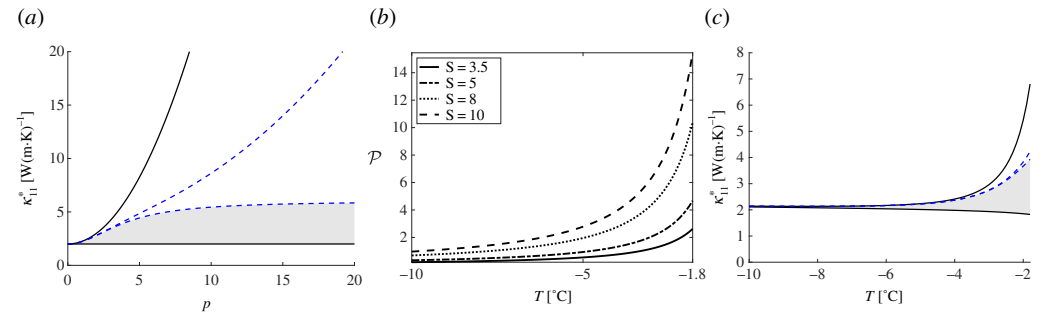


**Figure 3.** (a) Bounds on  $\kappa_{11}^*$  (W(m K) $^{-1}$ ) as a function of  $\mathcal{P}$ . Solid (black) lines form the first set of bounds (2.43), and dashed (blue) lines constitute the second set (2.44), with fixed  $\kappa=2$  (W(m K) $^{-1}$ ). (b) The Péclet number, plotted as a function of temperature, is illustrated for different values of salinity. Specifically, salinity values of  $S=\{3.5,5,8,10\}$  ppt correspond to solid, dash-dotted, dotted and dashed lines, respectively. Here, we fixed the parameters  $\upsilon=0.5\,\mathrm{m\,s^{-1}}$  and  $\rho=890\,\mathrm{kg\,m^{-3}}$ . (c) Bounds on  $\kappa_{11}^*$  (W(m K) $^{-1}$ ) as a function of T (°C). Solid lines (black) form the first set of bounds (2.43), and dashed lines (blue) constitute the second set (2.44), with fixed parameters  $S=5\,\mathrm{ppt}$ ,  $\upsilon=0.5\,\mathrm{m\,s^{-1}}$ ,  $\rho=890\,\mathrm{kg\,m^{-3}}$  and  $\mathcal{P}$  as defined in (3.6).

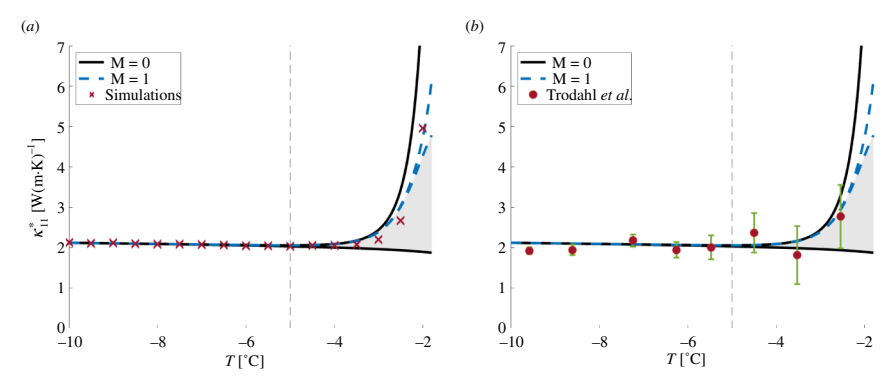


**Figure 4.** Bounds on  $\kappa_{11}^*$  as a function of temperature in the case of a BC fluid flow field. The solid (black) lines denote the first set of bounds as in (2.16) while the dashed (blue) lines denote the second set of bounds as in (2.17). The vertical dashed (grey) line denotes when  $T = -5^{\circ}$ C, roughly the critical temperature for percolation. (*a*) The *x*-dots (red) represent the numerical values of  $\kappa_{11}^*$  obtained by (4.7) for a BC flow as in (2.13). (*b*) The dots (red) denote the thermal conductivity data from [9] along with the accompanying error bars (green).

yield an integral representation for  $\kappa^*$  valid on the entire domain  $\Omega$ . This integral representation, given in terms of the Péclet number introduced in (2.5), can then be bounded. The Péclet number is a dimensionless parameter relevant to problems regarding transport phenomena and is constructed using the characteristic length of and velocity within  $\Omega_0$ . The fluid flow within the sea ice is represented by a BC flow or a cat's eye flow, resulting in similar bounds on  $\kappa^*$  given in (2.16)–(2.17) and (2.43)–(2.44), respectively. These are the first analytic bounds of the effective thermal conductivity in polar sea ice in the presence of convective fluid flow.

## (a) Mathematical background

Let  $\Omega \subset \mathbb{R}^d$  denote a domain filled by uniformed sea ice, and consider a spatially periodic sub-cell  $\Omega_0 \subset \Omega$ . Consider a mean-zero, incompressible, time-independent bulk fluid velocity field  $\mathbf{u}$  periodic on  $\Omega_0$ , satisfying  $\langle \mathbf{u} \rangle = 0$  and  $\nabla \cdot \mathbf{u} = 0$ , where  $\langle \cdot \rangle$  denotes spatial average over

 $\Omega_0$  (see figure 2c), where  $\Omega_0$  is a representative period cell for the uniformed sea ice. Let  $T(t, \mathbf{x})$  denote the temperature within sea ice at time  $t \ge 0$  and position  $\mathbf{x} \in \Omega_0$ , and  $\alpha$  is the constant thermal diffusivity of sea ice within a sub-cell  $\Omega_0$ . Given an initial temperature distribution  $T_0(\mathbf{x})$ , the temperature T satisfies the non-dimensionalized advection–diffusion equation

$$\frac{\partial T}{\partial t} = \alpha \Delta T + \mathbf{u} \cdot \nabla T, \qquad T(0, x) = T_0(x), \qquad t > 0, \qquad x \in \Omega_0.$$
 (2.1)

In this setting, we make the assumption that spatial variations of the initial temperature  $T_0$  occur on a spatial scale much larger than that for the bulk fluid flow  $\mathbf{u}$ . A rescaling of our problem in terms of fast variables, namely by letting  $t \mapsto t/\delta^2$  and  $\mathbf{x} \mapsto \mathbf{x}/\delta$  for some  $\delta \ll 1$ , allows us to study the long-time, large-scale solutions to this system through a temperature field  $\overline{T}$  defined by the limit [17,18,36–39]

$$\left\langle \int \left[ T \left( \frac{t}{\delta^2}, \frac{\mathbf{x}}{\delta} \right) - \overline{T}(t, \mathbf{x}) \right]^2 d\mathbf{x} \right\rangle \to 0 \quad \text{as } \delta \to 0.$$
 (2.2)

In particular,  $\overline{T}$  satisfies the diffusion equation [37,40,41]

$$\frac{\partial T}{\partial t} = \nabla \cdot (\boldsymbol{\alpha}^* \nabla \overline{T}), \quad \overline{T}(0, \boldsymbol{x}) = T_0(\boldsymbol{x}). \tag{2.3}$$

The constant, symmetric effective diffusivity tensor  $\alpha^*$  describes the long-time, large-scale thermal dispersion [42]. Using a spectral theorem for the self-adjoint operator  $i\Gamma \mathbf{H}\Gamma$  [34], where  $\Gamma = -\nabla(-\Delta)^{-1}\nabla$  is projection onto curl-free fields, and  $\mathbf{H}$  is the antisymmetric stream matrix associated with the fluid velocity field  $\mathbf{u}$  satisfying  $\mathbf{H}^T = -\mathbf{H}$  and  $\mathbf{u} = \nabla \cdot \mathbf{H}$ , the effective thermal conductivity  $\kappa^*$  can be explicitly represented as

$$\kappa^* = \kappa \left( I + \mathcal{P}^2 \int_{-\infty}^{\infty} \frac{\mathrm{d}\mu(\lambda)}{1 + \mathcal{P}^2 \lambda^2} \right). \tag{2.4}$$

with  $\kappa = \alpha \, c \rho$ , where c and  $\rho$  are the specific heat and the density of sea ice within  $\Omega_0$ , respectively. The matrix I denotes a  $d \times d$  identity matrix, and  $\mu$  is a tensor-valued measure whose components are spectral measures of the operator  $i\Gamma H\Gamma$  [17,34,35,43,44]. Here,  $\mathcal{P}$  is the *Péclet number*, or the comparative ratio of the magnitude of thermal convection to thermal diffusion, of the fluid flow field, defined in terms of the characteristic length  $L_c$ , characteristic velocity  $v_c$  and constant thermal diffusivity  $\alpha$  as [45]

$$\mathcal{P} = \frac{L_c v_c}{\alpha} \ . \tag{2.5}$$

The advection-dominated and diffusion-dominated regimes are characterized by  $\mathcal{P} \gg 1$  and  $\mathcal{P} \ll 1$ , respectively. The resulting integral representation (2.4), initially introduced in [17,44] for the effective thermal diffusivity, is known as a *Stieltjes integral*. It *separates* how the strength of the flow influences the effective behaviour from the geometry of the flow, such as the structure of convective cells or finer scale turbulent features, through  $\mathcal{P}$  and  $\mu$ , respectively.

Another advantage of the Stieltjes representation in (2.4) is that it can be written as a power series, allowing us to leverage the theory of Padé approximants, which are generalizations of power series expansions of functions that allow for approximation with only a finite number of terms. They can be used sometimes even when the power series fails to converge. To this end, we focus on a diagonal component of  $\kappa^*$  and write  $\kappa^* = \kappa_{jj}^*$  which involves the *positive* measure  $\mu = \mu_{jj}$ . We introduce the variable  $z = \mathcal{P}^2$  and rewrite  $\kappa^*$  in terms of the *Stieltjes function* f(z),

$$\kappa^* = \kappa(1 + zf(z)), \qquad f(z) = \int d\mu(\lambda)/(1 + z\lambda^2). \tag{2.6}$$

Expanding  $1/(1+z\lambda^2)$  in a geometric series leads to the following *Stieltjes series* representation of f(z) in involving the even moments  $\mu^{2n}$  of the spectral measure  $\mu$  [46],

$$f(z) = \int_{-\infty}^{\infty} \frac{d\mu(\lambda)}{1 + z\lambda^2} = \sum_{n=0}^{\infty} c_n z^n, \qquad c_n = (-1)^n \mu^{(2n)}, \qquad \mu^{(n)} = \int_{-\infty}^{\infty} \lambda^n d\mu(\lambda).$$
 (2.7)

The Padé approximant of order [L/M] of f(z) is given by

$$[L/M](z) = \frac{P^{[L/M]}(z)}{Q^{[L/M]}(z)},$$
(2.8)

where we define the determinants

$$P^{[L/M]}(z) = \begin{pmatrix} c_{L-M+1} & c_{L-M+2} & \cdots & c_{L+1} \\ c_{L-M+2} & c_{L-M+3} & \cdots & c_{L+2} \\ \vdots & \vdots & \ddots & \vdots \\ c_{L} & c_{L+1} & \cdots & c_{L+M} \\ \sum_{n=0}^{L-M} c_{n} z^{M+n} & \sum_{n=0}^{L-M+1} c_{n} z^{M+n-1} & \cdots & \sum_{n=0}^{L} c_{n} z^{n} \\ \end{pmatrix}, Q^{[L/M]}(z) = \begin{pmatrix} c_{L-M+1} & c_{L-M+2} & \cdots & c_{L} \\ c_{L-M+2} & c_{L-M+3} & \cdots & c_{L+1} \\ \vdots & \vdots & \ddots & \vdots \\ c_{L} & c_{L+1} & \cdots & c_{L+M-1} \\ z^{M} & z^{M-1} & \cdots & 1 \end{pmatrix},$$

using the convention that  $c_n = 0$  for n < 0 [46]. Padé approximants provide nested upper and lower bounds for the Stieltjes function f(z) when a finite number of the constants  $c_n$  are known. As more of the  $c_n$  are incorporated, the bounds become tighter and can converge in a region near z = 0. Specifically, the sequences  $\{[M-1/M]\}_{M=1}^{\infty}$  and  $\{[M/M]\}_{M=1}^{\infty}$  form nested, converging lower and upper bounds for f(z) in M, respectively [46]. Namely, for all  $M \ge 0$ ,

$$[-1/0](z) \le [0/1](z) \le \dots \le [M-1/M](z) \le f(z) \le [M/M](z) \le \dots \le [1/1](z) \le [0/0](z). \tag{2.9}$$

Applying the Padé approximants (2.9) to the Stieltjes function in (2.6) yields nested converging bounds on the components of the effective thermal conductivity  $\kappa^*$  of the form

$$\kappa (1 + \mathcal{P}^2[M - 1/M](z)) \le \kappa^* \le \kappa (1 + \mathcal{P}^2[M/M](z)), \qquad M \ge 0.$$
 (2.10)

The Padé approximants in (2.8) are given explicitly in terms of the  $c_n = (-1)^n \mu^{(2n)}$ .

One of the key difficulties in utilizing Padé approximant theory lies in computing explicit expressions for the moments  $\mu^{(n)}$ , as defined in (2.7), which depend on the convective flow within the system. It has been established for certain flow types, such as shear flow and flows mimicking confocal sphere assemblages, that the spectral measure can be explicitly computed and the values of  $\kappa^*$  attain Padé bounds. For example, the spectral measure for shear flow is given by a delta function centred at the spectral origin, so all the measure moments are zero except for the zeroth moment. In this case, the value for  $\kappa^*$  attains the upper bound [0/0](z) [17]. However, the nature of the brine flows through the porous microstructure of sea ice is more complex and not adequately represented by such flows. A more realistic model would be a periodic convective fluid with a wide up and a narrow down flow, as described in [23].

We now outline the method introduced in [33,34] and [35] to calculate the moments of the spectral measure. In principle, this method can be used to explicitly calculate *all* of the moments  $\mu^{(n)}$  of the spectral measure given any space–time periodic bulk velocity field expressible by a finite Fourier series of linear combinations of complex exponentials  $e^{i(\mathbf{k}\cdot\mathbf{x}+\omega t)}$ ,  $\mathbf{x}\in\Omega_0$ ,  $\mathbf{k}\in\mathbb{Z}^d$ ,  $\omega\in\mathbb{Z}$ . Specifically, for a given domain  $\Omega_0=[0,2\pi]^d$ ,  $d\geq 1$ , it was shown that for a non-dimensional mean-zero incompressible  $\Omega_0$ -periodic time-independent

fluid flow  $\mathbf{v} = (v_1, \dots, v_d)$ , which can be expressed as a linear combination of the functions  $e^{i\mathbf{k} \cdot \mathbf{x}}$ , the components of the moment  $\boldsymbol{\mu}^{(n)}$  take the form

$$\mu_{jk}^{(0)} = \left\langle g_{j}, g_{k} \right\rangle_{1, 2}, \quad \mu_{jk}^{(n)} = \left\langle \left[ i(-\Delta)^{-1} (\boldsymbol{v} \cdot \nabla) \right]^{n} g_{j}, g_{k} \right\rangle_{1, 2}, \quad g_{j} = (-\Delta)^{-1} v_{j}, \quad j, k = 1, ..., d, \tag{2.11}$$

involving the sesquilinear inner product  $\langle \phi, \psi \rangle_{1,2} = \langle \nabla \phi \cdot \overline{\nabla \psi} \rangle$  where  $\langle \cdot \rangle$  denotes the spatial average over  $\Omega_0$  and  $\overline{\psi}$  denotes the complex conjugate. Moreover, all the odd moments are zero, i.e.  $\mu^{(2n-1)} \equiv 0$  [17,34,35,43,44,47], whereas the components of the even moments  $\mu^{(2n)}$  are given by

$$\mu_{ik}^{(2n)} = \langle (\boldsymbol{v} \cdot \nabla)[(-\Delta)^{-1}(\boldsymbol{v} \cdot \nabla)]^{n-1}g_{i}, [(-\Delta)^{-1}(\boldsymbol{v} \cdot \nabla)]^{n}g_{k}\rangle_{2}, \tag{2.12}$$

where  $\langle \cdot, \cdot \rangle_2$  is the  $L^2(\Omega_0)$  inner product [34]. Since the  $v_j$  are given by a finite linear combination of the complex exponentials  $e^{ik \cdot x}$  and such exponentials are eigenfunctions of both of the operators  $(-\Delta)^{-1}$  and  $\nabla$ , the  $g_j$  are known explicitly, hence the  $[(-\Delta)^{-1}(\boldsymbol{v} \cdot \nabla)]^n g_j$  are known explicitly for each  $n = 1, 2, 3, \ldots$  Consequently, the orthogonality properties of complex exponentials can be used to explicitly compute  $\boldsymbol{\mu}^{(2n)}$  for each  $n = 1, 2, 3, \ldots$ 

#### (b) Analytic derivation of bounds on $\kappa^*$

Downloaded from https://royalsocietypublishing.org/ on 30 August 2024

In this study, we aim to integrate the previously derived results described above to establish upper and lower bounds on the non-zero components of the effective thermal conductivity  $\kappa^*$  of sea ice when convective brine flow is present. We consider the period domain  $\Omega_0 = [0, 2\pi]^2$  filled with a bulk brine velocity field  $\mathbf{u} = u_0 \mathbf{v}$ , where the constant  $u_0 \in (0, \infty)$  represents the strength of the flow, has dimensions of velocity (m s<sup>-1</sup>), and is independent of the flow geometry. The flow geometry is determined by the non-dimensional vector field  $\mathbf{v}$ , which is chosen to be either a BC flow of the form [48]

$$\mathbf{v} = (C\cos(x_2), B\cos(x_1)), \quad \mathbf{x} = (x_1, x_2) \in \Omega_0,$$
 (2.13)

for given  $B, C \in [0,1]$ , or a cat's eye flow of the form [18]

$$\mathbf{v} = (-\sin(x_1)\cos(x_2) + \beta\cos(x_1)\sin(x_2), \cos(x_1)\sin(x_2) - \beta\sin(x_1)\cos(x_2)), \tag{2.14}$$

for  $\mathbf{x} = (x_1, x_2) \in \Omega_0$  and a given  $\beta \in [-1,1]$ . Figure 1*c* depicts a cat's eye flow pattern. For both choices of flow geometry  $\mathbf{v}$ , the bulk brine velocity field  $\mathbf{u}$  is both divergence-free and mean-zero. With this choice of  $\mathbf{u}$  on a period sub-cell  $\Omega_0$ , the Péclet number  $\mathcal{P}$  appearing in (2.4) is determined by the strength of the flow  $v_c = u_0$  and the length  $L_c = 2\pi$  of a period sub-cell  $\Omega_0$ , and takes the form

$$\mathcal{P} = \frac{2\pi u_0}{\alpha} \ . \tag{2.15}$$

Next, we present and prove the key theorem of this paper, which establishes bounds on the effective thermal conductivity in terms of the Péclet number  $\mathcal{P}$ .

**Theorem 2.1.** Let  $\Omega_0 = [0, 2\pi]^2$  be a periodic domain with a bulk brine velocity field  $\mathbf{u}$ . If  $\mathbf{u} = u_0 \mathbf{v}$  with a non-dimensional BC flow geometry  $\mathbf{v}$  given in equation (2.13) with B, C  $\in$  [0,1], and dimensional flow strength  $u_0 > 0$ , then the effective thermal conductivity tensor  $\kappa^*$  is diagonal with entries  $\kappa_{11}^*$  and  $\kappa_{22}^*$ . Moreover, the first two sets of bounds on  $\kappa_{11}^*$  take the form

$$\kappa \le \kappa_{11}^* \le \kappa \left( 1 + \frac{C^2 \mathcal{P}^2}{2} \right), \tag{2.16}$$

$$\kappa \left( 1 + \frac{2C^2 \mathcal{P}^2}{4 + B^2 \mathcal{P}^2} \right) \le \kappa_{11}^* \le \kappa \left( 1 + \frac{40C^2 \mathcal{P}^2 + \left( 11C^4 - 9B^2C^2 \right) \mathcal{P}^4}{80 + 2\left( 11B^2 + C^2 \right) \mathcal{P}^2} \right), \tag{2.17}$$

where  $\mathcal{P}$  is the Péclet number and  $\kappa$  is the thermal conductivity of sea ice in the absence of fluid flow.

*Proof.* To obtain explicit expressions for the first two sets of bounds, for M = 0 and M = 1, we calculate the first three, non-zero moments of the measure  $\mu$ , and note that for the given BC flow  $\mathbf{v} = (v_1, v_2)$ , defined in (2.13), the following identities hold for j = 1, 2

$$g_i = v_i, \tag{2.18}$$

$$\mathbf{v} \cdot \nabla \mathbf{v}_{j} = \frac{-BC}{2} \left( \sin(x_{1} + x_{2}) + (-1)^{j} \sin(x_{1} - x_{2}) \right), \tag{2.19}$$

$$(-\Delta)^{-1} \left( \sin(x_1 + x_2) + (-1)^j \sin(x_1 - x_2) \right) = \frac{1}{2} \left( \sin(x_1 + x_2) + (-1)^j \sin(x_1 - x_2) \right). \tag{2.20}$$

Plugging (2.18) into (2.11), we establish that the zeroth moment  $\mu^{(0)}$  is diagonal and takes the form

$$\boldsymbol{\mu}^{(0)} = \frac{1}{2} \begin{pmatrix} C^2 & 0\\ 0 & B^2 \end{pmatrix}. \tag{2.21}$$

Combining (2.18)–(2.20) with (2.12) for n = 1, reduces the expression for the components of the second moment  $\mu^{(2)}$  to

$$\mu_{jk}^{(2)} = \langle \boldsymbol{v} \cdot \nabla v_{j}, (-\Delta)^{-1} (\boldsymbol{v} \cdot \nabla v_{k}) \rangle_{2}, \tag{2.22}$$

and direct calculations shows that  $\mu^{(2)}$  is diagonal and takes the form

$$\mu^{(2)} = \frac{B^2 C^2}{8} I,\tag{2.23}$$

where *I* is a 2 × 2 identity matrix. Following similar calculations, the fourth moment  $\mu^{(4)}$  takes the form

$$\boldsymbol{\mu}^{(4)} = \frac{B^2 C^2}{320} \begin{pmatrix} 11B^2 + C^2 & 0\\ 0 & 11C^2 + B^2 \end{pmatrix}. \tag{2.24}$$

Plugging the (1,1) entries of the moments  $\mu^{(n)}$ , n = 0, 2, 4, calculated in (2.21), (2.23) and (2.24), back into the Padé bounds framework (2.7)–(2.9), allows us to obtain the first two sets of nested approximants for M = 0,1

$$[-1/0](\mathcal{P}) = 0, \qquad [0/0](\mathcal{P}) = \frac{C^2}{2},$$

$$[0/1](\mathcal{P}) = \frac{2C^2}{4 + B^2 \mathcal{P}^2}, \qquad [1/1](\mathcal{P}) = \frac{40C^2 + (11C^4 - 9B^2C^2)\mathcal{P}^2}{80 + 2(11B^2 + C^2)\mathcal{P}^2},$$
(2.25)

which together with (2.10) yields the bounds on  $\kappa_{11}^*$  (2.16) and (2.17).

**Note 1.** Plugging the (2,2) entries of the moments  $\mu^{(n)}$ , n = 0, 2, 4, calculated in (2.21), (2.23) and (2.24), back into the Padé bounds framework (2.7)–(2.9), allows us to obtain the first two sets of Padé approximant bounds on  $\kappa_{22}^*$ , which are explicitly given by interchanging the roles of B and C in (2.16) and (2.17).

Acquiring bounds on the effective thermal conductivity while accounting for BC flow is a fundamental step towards establishing bounds on the effective thermal conductivity of sea ice under more intricate flow conditions. Specifically, by leveraging the bounds obtained in

royalsocietypublishing.org/journal/rspa Proc. R. Soc. A 480: 20230747

theorem (2.1) for BC flow, we can employ linear transformation techniques to deduce bounds on the effective thermal conductivity in scenarios involving cat's eye flow.

**Theorem 2.2.** Consider a periodic domain  $\Omega_0 \subset \mathbb{R}^d$ ,  $d \geq 1$ . Every cat's eye flow  $\tilde{\mathbf{u}}$  of the form (2.14) on  $\Omega_0$  can be written as a linear transformation of a BC flow  $\mathbf{u}$  of the form (2.13) on a new domain  $\tilde{\Omega}_0$ , which can be written as a linear transformation of  $\Omega_0$ . Moreover, the corresponding moments  $\tilde{\boldsymbol{\mu}}^{(n)}$  of the spectral measure  $\tilde{\boldsymbol{\mu}}$  as in (2.11) can be recovered through the corresponding spectral moments  $\boldsymbol{\mu}^{(n)}$  of the spectral measure for the associated BC flow via the relation

$$\widetilde{\mu}_{jk}^{(2n)} = \frac{1}{2} \left( \mu_{11}^{(2n)} + (-1)^{j+k} \mu_{22}^{(2n)} \right). \tag{2.26}$$

*Proof.* Let  $(x_1, x_2) \in \Omega_0$  and consider a general cat's eye flow for  $\beta \in [-1,1]$ 

$$\tilde{\mathbf{u}} = (-\sin(x_1)\cos(x_2) + \beta\cos(x_1)\sin(x_2), \cos(x_1)\sin(x_2) - \beta\sin(x_1)\cos(x_2)). \tag{2.27}$$

Using trigonometric identities, (2.27) reduces to

$$\widetilde{\mathbf{u}} = (B\cos(\theta_1) + C\cos(\theta_2), C\cos(\theta_2) - B\cos(\theta_1)), \tag{2.28}$$

where we introduce the constants  $B = \frac{1-\beta}{2}$  and  $C = \frac{1+\beta}{2}$ . The arguments  $\theta_1$ ,  $\theta_2$  can be expressed in terms of  $x_1$ ,  $x_2$  such that

$$\theta = (\theta_1, \theta_2) = \left(x_1 + x_2 + \frac{\pi}{2}, x_1 - x_2 + \frac{\pi}{2}\right). \tag{2.29}$$

Equation (2.28) allows us to express the cat's eye flow (2.27) as a linear transformation of a BC flow, i.e.

$$\widetilde{\mathbf{u}} = \begin{pmatrix} 1 & 1 \\ 1 & -1 \end{pmatrix} \begin{pmatrix} C\cos(\theta_2) \\ B\cos(\theta_1) \end{pmatrix}. \tag{2.30}$$

The moments of the measure for an admissible flow are defined in (2.12), specifically, for the cat's eye flow, we explicitly write

$$\widetilde{\mu}_{jk}^{(2n)} = \left\langle (\widetilde{\mathbf{u}} \cdot \nabla_{\mathbf{x}}) \left[ (-\Delta_{\mathbf{x}})^{-1} (\widetilde{\mathbf{u}} \cdot \nabla_{\mathbf{x}}) \right]^{n-1} g_{j} \left[ (-\Delta_{\mathbf{x}})^{-1} (\widetilde{\mathbf{u}} \cdot \nabla_{\mathbf{x}}) \right]^{n} g_{k} \right\rangle_{2}. \tag{2.31}$$

The linear transformation defined in equations (2.29)–(2.30) yields the relations

$$\widetilde{\mathbf{u}} \cdot \nabla_{\mathbf{x}} = \frac{1}{2} \mathbf{u} \cdot \nabla_{\theta}, \qquad (-\Delta_{\mathbf{x}})^{-1} = 2(-\Delta_{\theta})^{-1},$$
 (2.32)

and the expressions for cat's eye flow of  $\tilde{g}_j = (-\Delta)^{-1}\tilde{\mathbf{u}}$ , j = 1, 2 in (2.12) in terms of the BC flow,  $g_j = (-\Delta)^{-1}\mathbf{u}$  take the form

$$\tilde{g}_j = (g_1 + (-1)^{j+1} g_2).$$
 (2.33)

Plugging (2.32) and (2.33) back into (2.31) yields

$$\widetilde{\mu}_{jk}^{(2n)} = \frac{1}{2} \left\langle (\mathbf{u} \cdot \nabla_{\theta}) \left[ (-\Delta_{\theta})^{-1} (\mathbf{u} \cdot \nabla_{\theta}) \right]^{n-1} \left( g_1 + (-1)^{j+1} g_2 \right), \left[ (-\Delta_{\theta})^{-1} (\mathbf{u} \cdot \nabla_{\theta}) \right]^n \left( g_1 + (-1)^{k+1} g_2 \right) \right\rangle_2. \quad (2.34)$$

Using linearity (2.34) reduces to

by

$$\widetilde{\mu}_{jk}^{(2n)} = \frac{1}{2} \left( \mu_{11}^{(2n)} + (-1)^{j+k} \mu_{22}^{(2n)} \right),$$
(2.35)

where  $\mu_{11}^{(2n)}$  and  $\mu_{22}^{(2n)}$  diagonal entries of the  $\mu^{(2n)}$  moment for a BC flow, as found in theorem  $2.1_{\blacksquare}$ **Note 2.** Explicitly, the moments  $\tilde{\mu}^{(2n)}$  are symmetric and diagonally constant with components given

$$\widetilde{\mu}_{11}^{(2n)} = \widetilde{\mu}_{22}^{(2n)} = \frac{1}{2} (\mu_{11}^{(2n)} + \mu_{22}^{(2n)}),$$
(2.36)

$$\widetilde{\mu}_{12}^{(2n)} = \widetilde{\mu}_{21}^{(2n)} = \frac{1}{2} \left( \mu_{11}^{(2n)} - \mu_{22}^{(2n)} \right).$$
(2.37)

**Corollary 2.1.** For a cat's eye flow (2.14) with  $\beta = 0$  the moments take the form

$$\widetilde{\mu}^{(2n)} = \mu_{jj}^{(2n)} I, \qquad j = 1, 2.$$
(2.38)

*Proof.* Setting  $\beta = 0$  in the cat's eye flow (2.14), theorem 2.2 implies that B = C and theorem 2.1 implies  $\mu_{11}^{(2n)} = \mu_{22}^{(2n)}$ . Therefore, from equations (2.36)–(2.37) we conclude (2.38).

Using theorem 2.2 and the bounds in the case of BC flow from theorem 2.1, the below corollary follows directly:

**Corollary 2.2.** Let  $\Omega_0 = [0, 2\pi]^2$  be a periodic domain with a bulk brine velocity field **u**. If  $\mathbf{u} = u_0 \mathbf{v}$  with a non-dimensional cat's eye flow geometry  $\mathbf{v}$  given in equation (2.14) with  $\beta \in [-1,1]$ , and dimensional flow strength  $u_0 > 0$ , then the first two sets of nested Padé approximant bounds on the effective thermal conductivity  $\mathbf{x}^*$  take the form

$$\kappa I \leq \kappa^* \leq \kappa I \left( 1 + \frac{\mathcal{P}^2 (1 + \beta^2)}{8} \right),$$

$$\kappa I \left( 1 + \frac{2\mathcal{P}^2 (1 + \beta^2)^2}{16(1 + \beta^2) + \mathcal{P}^2 (1 - \beta^2)^2} \right) \leq \kappa^* \leq \kappa I \left( 1 + \frac{\mathcal{P}^2 (80(1 + \beta^2) + \mathcal{P}^2 (6(1 + \beta^2)^2 - 5(1 - \beta^2)^2))}{640 + 48\mathcal{P}^2 (1 + \beta^2)} \right), \tag{2.39}$$

where P is the Péclet number defined in (2.15),  $\kappa$  is the thermal conductivity of sea ice in the absence of fluid flow, and I is the  $2 \times 2$  identity matrix.

*Proof.* Plugging the moments (2.21), (2.23) and (2.24) from theorem 2.1, into (2.36) and (2.37), the moments of the measure for the case of a cat's eye flow, for n = 0, 2, 4, take the form

$$\mu^{(0)} = \begin{pmatrix} \frac{B^2 + C^2}{4} & \frac{C^2 - B^2}{4} \\ \frac{C^2 - B^2}{4} & \frac{B^2 + C^2}{4} \end{pmatrix}, \quad \mu^{(2)} = \begin{pmatrix} \frac{B^2 C^2}{8} & 0 \\ 0 & \frac{B^2 C^2}{8} \end{pmatrix},$$

$$\mu^{(4)} = \begin{pmatrix} \frac{3B^2 C^2 (B^2 + C^2)}{160} & \frac{B^2 C^2 (B^2 - C^2)}{64} \\ \frac{B^2 C^2 (B^2 - C^2)}{64} & \frac{3B^2 C^2 (B^2 + C^2)}{160} \end{pmatrix}, \quad (2.40)$$

or equivalently, in terms of  $\beta$ , where  $C = \frac{1+\beta}{2}$  and  $B = \frac{1-\beta}{2}$ ,

Downloaded from https://royalsocietypublishing.org/ on 30 August 2024

$$\mu^{(0)} = \begin{pmatrix} \frac{1+\beta^2}{8} & \frac{\beta^2}{4} \\ \frac{\beta^2}{4} & \frac{1+\beta^2}{8} \end{pmatrix}, \quad \mu^{(2)} = \begin{pmatrix} \frac{(1-\beta^2)^2}{128} & 0 \\ 0 & \frac{(1-\beta^2)^2}{128} \end{pmatrix},$$

$$\mu^{(4)} = \begin{pmatrix} \frac{3(1-\beta^2)^2(1+\beta^2)}{5120} & \frac{-\beta^2(1-\beta^2)^2}{1024} \\ \frac{-\beta^2(1-\beta^2)^2}{1024} & \frac{3(1-\beta^2)^2(1+\beta^2)}{5120} \end{pmatrix}.$$
(2.41)

The moments (2.41), and the Padé bounds framework (2.7)–(2.9), allow us to obtain the first two sets of nested approximants for M = 0.1

$$[-1/0](\mathcal{P}) = 0,$$

$$[0/0](\mathcal{P}) = \frac{1+\beta^2}{8},$$

$$[0/1](\mathcal{P}) = \frac{2(1+\beta^2)^2}{16(1+\beta^2) + \mathcal{P}^2(1-\beta^2)^2},$$

$$[1/1](\mathcal{P}) = \frac{80(1+\beta^2) + \mathcal{P}^2(6(1+\beta^2)^2 - 5(1-\beta^2)^2)}{640 + 48\mathcal{P}^2(1+\beta^2)}.$$
(2.42)

Plugging the approximants in (2.42) back into (2.10) yields the bounds in (2.39).

Having established bounds on the effective thermal conductivity in the case of the cat's eye flow using the linear transformation applied to a BC flow, we proceed to validate these bounds by a direct derivation of the aforementioned bounds for the cat's eye flow. For simplicity, we consider the case of a cat's eye flow with  $\beta = 0$ . The derivation of the bounds in the general case,  $\beta \in [-1,1]$ , follows a similar approach.

**Lemma 1.** Let  $\Omega_0 = [0, 2\pi]^2$  be a periodic domain with a bulk brine velocity field  $\mathbf{u}$ . If  $\mathbf{u} = u_0 \mathbf{v}$  with a non-dimensional cat's eye flow geometry  $\mathbf{v}$  given in equation (2.14) with  $\beta = 0$ , and dimensional flow strength  $u_0 > 0$ , then the effective thermal conductivity tensor  $\kappa^*$  is diagonal. Moreover, the first two sets of bounds on  $\kappa^*$  take the form

$$\kappa I \leq \kappa^* \leq \kappa I \left( 1 + \frac{\mathcal{P}^2}{8} \right), \tag{2.43}$$

$$\kappa I \left( 1 + \frac{2\mathcal{P}^2}{16 + \mathcal{P}^2} \right) \le \kappa^* \le \kappa I \left( 1 + \frac{\mathcal{P}^2 (80 + \mathcal{P}^2)}{640 + 48\mathcal{P}^2} \right),$$
(2.44)

where  $\mathcal{P}$  is the Péclet number defined in (2.15),  $\kappa$  is the thermal conductivity of sea ice in the absence of fluid flow, and I is the  $2 \times 2$  identity matrix.

*Proof.* We first note that for cat's eye flow  $\mathbf{v}$ , defined in (2.14) with  $\beta = 0$ , the following identities hold

$$g_j = \frac{1}{2}v_j, \quad \mathbf{v} \cdot \nabla v_j = \frac{1}{2}\sin(2x_j), \quad (-\Delta)^{-1}\sin(2x_j) = \frac{1}{4}\sin(2x_j),$$
 (2.45)

where  $v_j$  is the jth component of  $\boldsymbol{v}$ , j = 1,2. To obtain an explicit expression for the moments  $\boldsymbol{\mu}^{(n)}$ , n = 0, 2, 4, we combine (2.45) with (2.11) and (2.12), which yields

$$\mu^{(0)} = \frac{1}{8}I, \qquad \mu^{(2)} = \frac{1}{128}I, \qquad \mu^{(4)} = \frac{3}{5120}I,$$
(2.46)

where I is the 2 × 2 identity matrix. Plugging (2.46) back into the Padé bounds framework (2.7)–(2.9), allows us to obtain the first two sets of nested approximants for M = 0,1

$$[-1/0](\mathcal{P}) = 0$$
,  $[0/0](\mathcal{P}) = \frac{1}{8}$ ,  $[0/1](\mathcal{P}) = \frac{2}{16 + \mathcal{P}^2}$ ,  $[1/1](\mathcal{P}) = \frac{80 + \mathcal{P}^2}{640 + 48\mathcal{P}^2}$ ,  $(2.47)$ 

which, combined with (2.10) yield the bounds in (2.43) and (2.44).

Downloaded from https://royalsocietypublishing.org/ on 30 August 2024

Given the thermal conductivity of sea ice in the absence of fluid flow  $\kappa$ , theorem 2.1 and lemma 1 provide bounds on the effective thermal conductivity  $\kappa^*$  as a function of Péclet number, assuming the convective flow field has a BC or cat's eye geometry, respectively. Figure 3a depicts the two sets of bounds (2.43) (black/solid lines) and (2.44) (blue/dashed lines) as a function of  $\mathcal P$  when  $\kappa$  is a fixed constant. While these bounds cannot be directly compared with in situ data, the gap between the lower solid (black) bound, which is independent of convective flow, and the lower dashed (blue)

royalsocietypublishing.org/journal/rspa *Proc. R. Soc. A* **480:** 20230747

bound, which incorporates the sub-cell flow strength, guarantees the enhancement in effective thermal conductivity.

**Note 3.** The analysis in this section addresses the transport of a passive tracer within porous media and is applicable outside the scope of sea ice.

In situ measurements of the effective thermal conductivity of sea ice  $\kappa^*$  are usually reported as a function of temperature T, it is necessary to convert the analytic bounds found in this section to a temperature-dependent form for comparison with available data. For this purpose, in the following section, we will broaden our perspective and concentrate on sea ice properties in a macroscale framework, over  $\Omega$ . This will allow us to understand the properties of sea ice at a larger scale and provide a comprehensive overview of the behaviour of the effective thermal conductivity under varying conditions.

# 3. Bounds as a function of temperature

In §2, we considered sea ice as a porous medium and derived bounds for the effective thermal conductivity  $\kappa^*$  in the presence of a periodic bulk convective fluid flow as a function of the Péclet number. While the Péclet number plays an important role in the theory of fluid flow within porous media, measurements of the effective thermal conductivity of sea ice are often given as a function of temperature. To compare the bounds found in §2 with available in situ effective thermal conductivity data, it is necessary to convert them into a temperature-dependent form. The effective thermal conductivity  $\kappa^*$  is a macroscale material property of sea ice, and yet the bounds we derived depend on the microscale properties defined locally within a sub-cell  $\Omega_0$ , such as the thermal conductivity  $\kappa$  and the Péclet number  $\mathcal{P}$ . Within  $\Omega_0$ , the thermal conductivity  $\kappa$  is constant, and the representation of the Péclet number (2.15) given in §2 involves the strength  $u_0$  of the prescribed fluid flow. In this section, we will take into account the entire domain  $\Omega$  on which the properties depend on both temperature and salinity. Moreover, we will reconsider the general representation for the Péclet number (2.5), derive a specific form for  $\mathcal{P}$  on  $\Omega$  and reveal the relation between the local flow strength  $u_0$  and the Darcy velocity within the sea ice. This will enable us to connect the analytic bounds with the physical nature of the problem, extending the bounds presented in §2 in terms of macroscale properties of sea ice. To this end, we will review the physical and thermal properties of sea ice as a function of both temperature *T* and salinity *S*.

### (a) Sea ice physical and thermal properties

In the context of sea ice, the permeability is governed by the brine volume fraction, which changes with temperature T (°C) and salinity S (ppt). In particular, for  $T \in [-22.9, -0.5]$ °C, the brine volume fraction  $\phi$  is given by [49]

$$\phi = \frac{S}{1000} \left( \frac{49.185}{|T|} + 0.532 \right),\tag{3.1}$$

and the sea ice permeability  $\Pi(m^2)$  satisfies the relation [50]

$$\Pi(\phi) = 3\phi^3 \times 10^{-8} \ . \tag{3.2}$$

The thermal properties of sea ice *without* the presence of fluid flow, also depend on temperature and salinity. In particular, the thermal conductivity of sea ice without fluid flow  $\kappa$  (W (m K)<sup>-1</sup>) is given by the BB model [8] as

$$\kappa = \frac{\rho}{\rho_i} \left( 2.11 - 0.011T + 0.09 \frac{S}{T} \right),\tag{3.3}$$

where  $\rho$  and  $\rho_i$  are the density (kg m<sup>-3</sup>) of sea ice and pure ice, respectively, or by the MU71 model [12] as

$$\kappa = 2.03 + 0.117 \frac{S}{T} \ . \tag{3.4}$$

For the range of sea ice densities  $\rho$  which are physically relevant (see table 1), the absolute error between the two representations of  $\kappa$  in (3.3) and (3.4) is at most  $O(10^{-1})$ , and without loss of generality we choose to use the BB model (3.3) for the rest of this paper.

The specific heat capacity c (J (kg K)<sup>-1</sup>), for temperatures between  $-1.8^{\circ}$ C and  $-23^{\circ}$ C, takes the form [2,24]

$$c = 4186.8 \left( 0.505 + 0.0018T - 0.0008S + 0.000019ST + 4.3115 \frac{S}{T^2} \right). \tag{3.5}$$

Refer to table 1 for a concise overview of the parameters discussed in this section.

#### (b) Péclet number for sea ice

Utilizing the provided sea ice data, we establish a relationship between the Péclet number in  $\Omega$  and temperature, which is formally presented in the subsequent lemma.

**Lemma 2.** Let  $\Omega \in \mathbb{R}^d$  be a domain of uniformed sea ice. The Péclet number of sea ice  $\mathcal{P}(S, T)$  in  $\Omega$  as a function of salinity S (ppt) and temperature  $T(^{\circ}C)$  takes the form

$$\mathcal{P}(S,T) = \sqrt{3}v \frac{c\rho\phi^{3/2}}{\kappa} \cdot 10^{-4},\tag{3.6}$$

where v is the Darcy velocity,  $\phi$  is the brine volume fraction (3.1), c is the specific heat capacity (3.5),  $\rho$  is the density of sea ice and  $\kappa$  is the thermal conductivity of sea ice without fluid flow.

*Proof of lemma* 2. We introduced the general form of  $\mathcal{P}$  in (2.15) in terms of a characteristic length  $L_c$  and a characteristic velocity  $v_c$ . On the domain  $\Omega$ , the characteristic length is the square root of the permeability [52], and the characteristic velocity is the Darcy velocity. Thus, the Péclet number on this scale is parametrized as

$$\mathcal{P} = \frac{\sqrt{\Pi}v}{\alpha},\tag{3.7}$$

where  $\Pi$  is the fluid permeability as defined in (3.2),  $\alpha$  is the thermal diffusivity, and v is the Darcy velocity, which is assumed to be approximately  $O(10^{-1})$  (m s<sup>-1</sup>). Fluid velocities of this order of magnitude are likely to be in the upper range of or even above what may be attainable in natural sea ice but serve to demonstrate how significant advective enhancement can be in sea ice thermal transport. This parametrization is, indeed, one of several versions of the Péclet number applicable to the study of porous materials [53–55], and it is particularly relevant in the case of sea ice when considered as a saturated rock. Plugging (3.2) back into (3.7) and using the relation  $\kappa = \alpha c \rho$  yields the required result (3.6).

The representation for the Péclet number in (3.7), in conjunction with that in (2.15), allows us to make sense of both the strength  $u_0$  of our prescribed convective bulk flow and the length scale of the dimensionless sub-cell problem. In (2.15), we considered a non-dimensionalized advection–diffusion equation within the mathematically abstracted period sub-cell  $\Omega_0$ , where the characteristic length  $L_c = 2\pi$  and velocity  $v_c = u_0$  were naturally associated. In (3.7) we considered a dimensionalized advection–diffusion throughout the full physical material on the domain  $\Omega$  with characteristic length  $L_c = \sqrt{\Pi}$  and velocity  $v_c = v$ . To connect the two settings of our problem, we equate the two representations for the Péclet number and find that

**Table 1.** Table of parameters.

symbol	description	value	units
$\mathcal{P}$	Péclet number		_
υ	Darcy velocity	$10^{-1} - 10^{-2}$	m s <sup>-1</sup>
П	permeability	$10^{-8} - 10^{-11}$ [51]	m²
φ	brine volume fraction	(0,1]	<del>-</del>
α	diffusion coefficient	$O(10^{-7})$	$\mathrm{m}^2\mathrm{s}^{-1}$
κ	conductivity coefficient without flow		W (m K)⁻¹
С	specific heat capacity		J (kg K) <sup>-1</sup>
S	salinity	[0,10]	ppt
ρ	sea ice density	[840,940] [8]	kg m <sup>-3</sup>
$ ho_i$	pure ice density	917	kg m <sup>−3</sup>
T	temperature	[-22.9, -1.8]	°C

$$u_0 = \frac{\sqrt{\Pi}}{2\pi} v . \tag{3.8}$$

We conclude that the dimensionless length scale for the sub-cell problem,  $2\pi$ , should be of the order of  $\sqrt{\Pi}$ , where  $\Pi$  is defined in (3.2), for this relation to hold. With this relationship, we expect that as the permeability, and thus the brine volume fraction, of the sea ice increases, the strength of the prescribed convective flow in  $\Omega_0$  also increases. This relationship also consolidates our understanding of the two definitions we use for the Péclet number. In particular, (2.15) provides a representation of the Péclet number when the problem is viewed in the mathematically abstracted microscale as in (2.1), while (3.7) comes from a macroscale perspective of the physical system in which all properties defined in table 1 hold.

The behaviour of the Péclet number exhibits distinct characteristics with changing temperatures. At low temperatures, the Péclet number remains small, indicating a regime dominated by diffusion. However, as the temperature surpasses the percolation temperature and the sea ice becomes permeable, the Péclet number experiences a rapid increase. In particular, as the temperature approaches zero, the Péclet number becomes unbounded, as depicted in figure 3b. This transition signifies the shift from a diffusion-dominated regime at colder temperatures to an advection-dominated regime at warmer temperatures. These findings align with the concept of sea ice as a mushy layer, characterized by convective flow within the ice [15,19,20,22,56].

Incorporating the revised expression of the Péclet number, as given by (3.6), into the bounds derived in §2, allows us to bound the effective thermal conductivity as a function of temperature for a given fluid velocity field. Figure 3c depicts the bounds on the effective thermal conductivity of sea ice  $\kappa^*$  in the presence of a periodic cat's eye fluid flow as a function of temperature, as obtained by plugging  $\mathcal{P}(S,T)$  from (3.6) into the previously computed Padé bounds (2.43) and (2.44). The gap between the lower solid (black) bound, which is independent of convective flow, and the lower dashed (blue) bound, which incorporates the flow strength of the domain  $\Omega$ , guarantees the enhancement in effective thermal conductivity. Moreover, this dependency of the lower bound in (2.44) on the temperature implies that in the presence of flow, the effective thermal conductivity will increase and that values of the effective thermal conductivity used in large-scale sea ice and climate models without accounting for advection are probably well off from the correct values in those situations where a brine velocity field is

active. These bounds highlight the importance of accounting for this enhancement to improve accuracy in global climate models. Further, this corroborates the experimental findings of Trodahl *et al.* [9], who proposed an enhancement in thermal conductivity for temperatures beyond the critical temperature for percolation [13,50], due to the added convective flow, see figure 4b. To verify the analytical findings presented in §2 and §3, we will proceed with a numerical validation through the implementation of subsampling simulations.

## 4. Comparison of bounds with simulations and field data

In this section, we provide a quantitative validation for our analytic bounds by numerically estimating the diagonal elements of  $\kappa^*$ . The advection–diffusion equation (2.1) is the Fokker–Planck equation for the probability density of a random process governed by an SDE [57]. Leveraging this relationship, we employ the methods developed by Cotter and Pavliotis to estimate the effective thermal conductivity  $\kappa^*$  [58]. Additionally, we qualitatively compare our bounds with Antarctic field data, as reported in [9].

Introducing a scaled bulk fluid velocity field  $\hat{\mathbf{u}} = \hat{\mathbf{u}}(\mathbf{x}, \tau)$  at the position  $\mathbf{x}$  and time  $\tau$ , defined as  $\hat{\mathbf{u}} = c\rho\mathbf{u}$  and satisfying  $\nabla \cdot \hat{\mathbf{u}} = 0$ , and a change of variables  $t = c\rho\tau$ , the advection–diffusion (2.1) takes the form

$$\frac{\partial T}{\partial \tau} = \kappa \Delta T + \mathbf{\hat{u}} \cdot \nabla T, \tag{4.1}$$

where T is the temperature and  $\kappa$  is the uniform conductivity of sea ice in the absence of fluid flow. By considering T to be a probability density function, we can interpret (4.1) as a Fokker–Planck equation associated with an SDE. In particular, (4.1) corresponds to a Langevin equation of the form [48,57,59,60]

$$\frac{\mathrm{d}x}{\mathrm{d}\tau} = \hat{\mathbf{u}}(x(\tau), \tau) + \sqrt{2\kappa} \frac{\mathrm{d}W_{\tau}}{\mathrm{d}\tau},\tag{4.2}$$

where  $W_{\tau}$  is the Wiener process, or Brownian motion, with its time derivative  $\frac{dW_{\tau}}{d\tau}$  representing Gaussian white noise. Thus, the realization of a random process undergoing advection and diffusion,  $X_{\tau} = \mathbf{x}(\tau)$ , satisfies the Itô SDE

$$dX_{\tau} = \mathbf{\hat{u}}(X_{\tau}, \tau)d\tau + \sqrt{2\kappa} dW_{\tau}. \tag{4.3}$$

To obtain the behaviour of the effective thermal conductivity we introduce the rescaled random walk  $X_{\tau}^{\varepsilon} = \varepsilon X_{\tau}(\tau/\varepsilon^2)$ , and obtain the rescaled SDE

$$dX_{\tau} = \frac{1}{\epsilon} \hat{\mathbf{u}} \left( \frac{X_{\tau}}{\epsilon}, \tau \right) + \sqrt{2\kappa} \ dW_{\tau} \,. \tag{4.4}$$

Cotter & Pavliotis [58] showed that, for the time interval  $[0,\mathfrak{T}]$ , with  $\mathfrak{T} < \infty$  fixed, the scaled random walk  $X_{\tau}^{\varepsilon}$  converges weakly on  $C[[0,\mathfrak{T}];\mathbb{R}^2]$  to the Brownian motion

$$\lim_{\varepsilon \to 0} dX_{\tau}^{\varepsilon} = \sqrt{2\kappa^*} dW_{\tau}. \tag{4.5}$$

Furthermore, Cotter & Pavliotis [58] showed that *subsampling* is required to obtain an accurate expression for  $\kappa^*$ . We follow their method and present a brief summary of the method applied to our SDE (4.4) as follows. We let  $\kappa$  be a function of temperature as in (3.3) or (3.4). For  $\tau \in [0, \mathfrak{T}]$ , let  $\tau_m = m\Delta \tau$ , m = 0, ..., M, with  $\tau_0 = 0$ ,  $\tau_M = \mathfrak{T}$ , and for each realization n = 1, ..., N, the *Euler–Maruyama* method updates an initial condition  $x_{n,0} = X_0$  according to the recursive rule

$$x_{n,m+1} = x_{n,m} + \hat{\mathbf{u}}(x_{n,m}, \tau_m) \Delta \tau + \sqrt{2\kappa} \Delta w_{n,m}, \tag{4.6}$$

royalsocietypublishing.org/journal/rspa Proc. R. Soc. A 480: 20230747

$$\Delta w_{n,m} = w_{n,m+1} - w_{n,m}. \tag{4.7}$$

See [61] for additional details. The subsampling method requires us to consider displacement over time steps which are larger than  $\Delta \tau$ , and we estimate the conductivity using the quadratic variation

$$\kappa_{n,\delta\tau}^* = \frac{1}{2\mathfrak{T}} \sum_{k=0}^{K-1} (x_{n,k+1} - x_{n,k}) \otimes (x_{n,k+1} - x_{n,k}), \tag{4.8}$$

where  $x_{n,k}$  are approximate sample paths of (4.4) generated with a time step  $\delta \tau$  and subsampled at times  $\tau_k$ ,  $\{\tau_k: \tau_{k+1} = \tau_k + \delta \tau, \tau_0 = 0, \mathfrak{T} = K \delta \tau, k = 0, 1, \dots, K\}$  with  $\delta \tau > \Delta \tau$ . Moreover, Cotter & Pavliotis [58] showed that for  $\delta \tau = \epsilon^{\sigma}$  with  $\sigma \in (0,2)$ , the error estimate on  $\kappa_{n,\delta\tau}^*$  as in (4.7) is bounded.

In figure 4a, we present both our analytic bounds and numerical simulation results when  $\kappa$  is parametrized as in (3.3). We choose B = C = 0.5, S = 4 ppt, v = 0.1 m s<sup>-1</sup> and  $\rho = 890$  kg m<sup>-3</sup>. Here, we choose the numerical parameters to minimize the order of the error. In particular, we choose the time step  $\Delta \tau = 5 \times 10^{-4}$  with subsampling time step  $\delta \tau = 5 \times 10^{-3}$ . Each experiment ran for a sample size of N = 100, and a long time  $\mathfrak{T} = 1000$  to allow advective enhancement to stabilize. Initial positions of the random walk  $X_0$  were uniformly chosen in the domain  $\Omega_0 = [0, 2\pi]^2$ . Our simulation results quantitatively agree with the analytic bounds and capture a similar enhancement of the effective thermal conductivity.

In their study, Trodahl et al. [9] collected in situ measurements of the thermal conductivity of sea ice in Antarctica. Conducting measurements in such extreme conditions is challenging, where the error in the measurements increases with rising temperature and subsequent increase in sea ice permeability. Despite the large error in measurements, Trodahl et al. suggested that the observed enhancement in effective thermal conductivity at warmer temperatures is due to convective flow within the sea ice resulting from increased permeability of the sea ice. The analytic bounds derived in (2.16) and (2.17) support this argument, as the field data lies within our analytic bounds, see figure 4c. Furthermore, the region where the two lower bounds diverge implies that such enhancement is guaranteed.

**Note 4.** Figure 4 depicts the numerical values of  $\kappa_{11}^*$ . However, given the symmetry for  $\kappa^*$  when B=C, the values of  $\kappa_{22}^*$  are statistically the same. The case of B>C can better capture the anisotropy in sea ice, in which case  $\kappa_{11}^* \neq \kappa_{22}^*$ .

**Note 5.** Enhancement is guaranteed due to the gap between the two lower bounds for  $\kappa^*$ . The solid (black) lower bound represents the thermal conductivity without fluid flow  $\kappa$ , and the lower dashed (blue) bound is the first lower bound involving the fluid velocity field. This area is marked grey in figure 4.

#### 5. Conclusions

This paper presents a novel and rigorous mathematical framework for the characterization of enhanced thermal transport in porous composite materials, focusing specifically on the case of sea ice. Building upon previous theoretical advances [17,34,35,46], we have derived the first analytic bounds for the effective thermal conductivity of sea ice for two models of convective bulk fluid flows that provide an initial approximation of flow fields in sea ice. Our results establish that once a convective fluid flow is active in the sea ice, an enhancement is expected in the effective thermal conductivity. Furthermore, the analytic bounds demonstrate a close alignment with our numerical simulations, indicating that these techniques offer accurate estimates of effective thermal conductivity in diffusion-dominated fluid flows, such as those encountered in thermal transport through sea ice. Employing such convective fluid flows, while mathematically convenient and physically relevant, does not exhibit the full complexity of fluid exchange between the ocean and sea ice. When brine is rejected from the sea ice layer into the ocean, relatively fresh seawater enters the sea ice layer, impacting the temperature, salinity and fluid properties within the system. The detailed modelling of such feedback mechanisms is outside the scope of this paper. To overcome this difficulty, we assumed that the fluid flow is imposed on the system and does not experience interactions with the system. In other words, we assumed that the fluid flow is not affected by changes in temperature. Adopting a predetermined fluid flow field made our analysis presented in this paper feasible.

In situ measurements of the thermal conductivity of sea ice present significant challenges, leading to a scarcity of available data. Collecting these measurements under harsh and variable conditions requires sophisticated equipment and methodologies. Additionally, as temperatures increase and sea ice becomes permeable, the difficulty of accurately collecting such data increases. As a result, the most recent comprehensive in situ study of sea ice thermal conductivity was conducted nearly two decades ago [9,62]. This lapse in updated measurements is particularly relevant given the dynamic nature of sea ice. Recent years have witnessed a shift in the composition of sea ice, with an increase in first-year ice [63]. First-year ice has different physical properties compared with multi-year ice and, in particular, the brine rejection that occurs in first-year ice results in convective flow within the mushy layer, which enhances the thermal conductivity. In 2001, Trodahl et al. assumed an increase in thermal conductivity within sea ice at higher temperatures due to fluid flow, as per their measurements [9]. Our findings, derived from an analytical mathematical model, support this hypothesis. Although the empirical data from Trodahl et al. is subject to significant uncertainties, our results conclusively demonstrate that an enhancement in effective thermal conductivity is inevitable at warmer temperatures, where sea ice becomes permeable to fluid flow. This provides a theoretical underpinning to the observed phenomena, highlighting the critical role of temperature and fluid dynamics in the thermal properties of sea ice. Updated in situ measurements are required to accurately understand and predict the thermal dynamics of sea ice, especially in the context of global climate change and its impact on polar regions.

The results of this paper extend significantly into the realm of climate modelling, with the results indicating that the addition of convective flow within sea ice could cause the effective thermal conductivity to increase by a factor of roughly 2–3. This enhancement primarily applies to the lower, warmer section of the sea ice where temperature and permeability are sufficient for convection. During the freezing season, this effect is confined to the bottom 10 cm, and while full permeability may occur in summer, the vertical temperature gradients and resulting heat fluxes are much smaller. This finding suggests a potential underestimation in calculating heat flux by a similar factor in existing climate models. Global climate models might benefit from incorporating the bounds presented in this paper, which will, under certain conditions, allow them to capture the enhancement of thermal transport through sea ice in their models. Recognizing and addressing this discrepancy is crucial for increasing the accuracy of climate projections. The integration of a flexible, convective flow-dependent thermal conductivity mechanism into climate models could improve our understanding of sea ice dynamics and contribute to more precise predictions of ice growth and melt patterns, especially with rising temperatures.

The significance of this paper extends beyond the specific context of this study, indeed, to thermal transport through almost any porous medium where the pore space is filled with a fluid that can move. Our work here also applies to the bulk transport of other tracers through almost any porous medium. In sea ice, our results can, in principle, be applied to advection–diffusion of salt or nutrients being transported through the ice, as well as heat. Moreover, our methodology incorporates the Péclet number in the derivation of the bounds. As the Péclet number holds broad relevance for transport phenomena in materials with a porous microstructure, our results offer applicability to a broad range of systems beyond sea ice. Finally, while representations of the Péclet number as a function of physical properties of a given specific porous medium are available in the literature, this paper suggests the first physical representation of the Péclet number as a function of temperature and salinity in the

context of sea ice. While outside the scope of this paper, such a representation will allow us to relate the ratio of advection to diffusion with changes in temperature.

In conclusion, this research establishes a rigorous mathematical foundation for investigating and quantifying the enhanced thermal transport in composite materials, with a particular focus on sea ice. Our study provides valuable analytic bounds, validated through numerical simulations and field data, which serve as robust tools for characterizing effective thermal conductivity. Furthermore, these results provide an initial step towards understanding effective thermal conductivity in the presence of convective flow in sea ice. Future projects should try to fully capture the precise structure of the natural convective flow, incorporate variable processes inherent to the system, such as brine rejection, and capture the dependence of the fluid flow on heterogeneity and porous structure of the sea ice. In addition, the inclusion of melting and freezing processes, which affect the fluid flow properties, brine volume fraction and connectivity, can improve the estimated bounds. Further research aiming to refine the models to account for the detailed characteristics of convective flow will be vital to building on the bounds established in this study. The results we have presented will serve as a cornerstone for developing more accurate and realistic models of thermal transport in sea ice. Additional future directions involve validating our methods further with field data and integrating our results into climate models to enhance predictions related to polar sea ice and climate processes.

Data accessibility. The data are available from Zenodo [64].

Declaration of Al use. We have not used AI-assisted technologies in creating this article.

Authors' contributions. N.K.: conceptualization, formal analysis, project administration, supervision, validation, visualization, writing—review and editing; R.H.: data curation, formal analysis, investigation, software, validation, visualization, writing—original draft, writing—review and editing; H.D.: methodology, software, validation, visualization, writing—original draft; N.B.M.: conceptualization, formal analysis, investigation, methodology, software, supervision, validation, writing—original draft, writing—review and editing; E.C.: conceptualization, funding acquisition, investigation, methodology, supervision, validation, writing—review and editing; J.Z.: formal analysis, investigation, methodology, supervision, validation, writing—review and editing; K.M.G.: conceptualization, funding acquisition, investigation, methodology, project administration, supervision, validation, writing—review and editing.

All authors gave final approval for publication and agreed to be held accountable for the work performed therein.

Conflict of interest declaration. We declare we have no competing interests.

Funding. We are grateful for support from the Applied and Computational Analysis Program and the Arctic and Global Prediction Program at the US Office of Naval Research through grants N00014-12-1-0861, N00014-13-1-0291, N00014-18-1-2552, N00014-18-1-2041 and N00014-21-1-2909. We also gratefully acknowledge support from the Division of Mathematical Sciences at the US National Science Foundation (NSF) through grants DMS-0940249, DMS-1413454, DMS-213619, DMS-2136198, and DMS-2206171.

## References

Downloaded from https://royalsocietypublishing.org/ on 30 August 2024

- Kannuluik W, Carman E. 1951 The temperature dependence of the thermal conductivity of air. Aust. J. Chem. 4, 305. (doi:10.1071/CH9510305)
- Yen YC. 1981 Review of thermal properties of snow, ice, and sea ice. Technical Report 81-10. Hanover, NH: Cold Regions Research and Engineering Laboratory.
- 3. Thomas DN, Dieckmann GS. 2008 Sea ice: an introduction to its physics, chemistry, biology and geology. Berlin, Germany: John Wiley & Sons.
- Semtner AJ. 1976 A model for the thermodynamic growth of sea ice in numerical investigations of climate. J. Phys. Oceanogr. 6, 379–389. (doi:10.1175/1520-0485(1976)006
   0379:AMFTTG>2.0.CO;2)
- 5. Weeks WF, Ackley SF. 1986 The growth, structure, and properties of sea ice. In *The geophysics of sea ice*, pp. 9–164. Boston, MA: Springer. (doi:10.1007/978-1-4899-5352-0\_2)

- Hanesiak JM, Barber DG, Flato GM. 1999 Role of diurnal processes in the seasonal evolution of sea ice and its snow cover. J. Geophys. Res. 104, 13593–13603. (doi:10.1029/1999JC900054)
- Lemke P, Hibler WD, Flato G, Harder M, Kreyscher M. 1997 On the improvement of sea-ice models for climate simulations: the sea ice model intercomparison project. A. Glaciology 25, 183–187. (doi:10.1017/S0260305500014002)
- 8. Pringle DJ, Eicken H, Trodahl HJ, Backstrom LGE. 2007 Thermal conductivity of landfast Antarctic and Arctic sea ice. *J. Geophys. Res.* **112**, C04017. (doi:10.1029/2006JC003641)
- Trodahl HJ, Wilkinson SOF, McGuinness MJ, Haskell TG. 2001 Thermal conductivity of sea ice; dependence on temperature and depth. *Geophys. Res. Lett.* 28, 1279–1282. (doi:10.1029/ 2000GL012088)
- 10. Voldoire A *et al.* 2013 The CNRM-CM5.1 global climate model: description and basic evaluation. *Clim. Dyn.* 40, 2091–2121. (doi:10.1007/s00382-011-1259-y)
- 11. Kiss AE *et al.* 2020 ACCESS-OM2 v1.0: a global ocean–sea ice model at three resolutions. *Geosci. Model Dev.* **13**, 401–442. (doi:10.5194/gmd-13-401-2020)
- 12. Maykut GA, Untersteiner N. 1971 Some results from a time-dependent thermodynamic model of sea ice. *J. Geophys. Res.* **76**, 1550–1575. (doi:10.1029/JC076i006p01550)
- 13. Golden KM, Ackley S, Lytle V. 1998 The percolation phase transition in sea ice. *Science* **282**, 2238–2241. (doi:10.1126/science.282.5397.2238)
- Fritsen CH, Lytle VI, Ackley SF, Sullivan CW. 1994 Autumn bloom of Antarctic pack-ice algae. Science 266, 782–784. (doi:10.1126/science.266.5186.782)
- 15. Worster MG, Wettlaufer JS. 1997 Natural convection, solute trapping, and channel formation during solidification of saltwater. *J. Phys. Chem. B* **101**, 6132–6136. (doi:10.1021/jp9632448)
- 16. Wettlaufer JS, Worster MG, Huppert HE. 1997 Natural convection during solidification of an alloy from above with application to the evolution of sea ice. *J. Fluid Mech.* **344**, 291–316. (doi:10.1017/S0022112097006022)
- 17. Avellaneda M, Majda AJ. 1991 An integral representation and bounds on the effective diffusivity in passive advection by laminar and turbulent flows. *Commun. Math. Phys.* **138**, 339–391. (doi:10.1007/BF02099496)
- Fannjiang A, Papanicolaou G. 1994 Convection enhanced diffusion for periodic flows. SIAM J. Appl. Math. 54, 333–408. (doi:10.1137/S0036139992236785)
- Wells AJ, Wettlaufer JS, Orszag SA. 2011 Brine fluxes from growing sea ice. *Geophys. Res. Lett.* 38, L04501. (doi:10.1029/2010GL046288)
- 20. Feltham DL, Worster MG, Wettlaufer JS. 2002 The influence of ocean flow on newly forming sea ice. *J. Geophys. Res. Ocean.* **107**, 1–1. (doi:10.1029/2000JC000559)
- 21. Feltham DL, Untersteiner N, Wettlaufer JS, Worster MG. 2006 Sea ice is a mushy layer. *Geophys. Res. Lett.* **33**, 14. (doi:10.1029/2006GL026290)
- 22. Worster MG, Rees Jones DW. 2015 Sea-ice thermodynamics and brine drainage. *Phil. Trans. R. Soc. A* **373**, 20140166. (doi:10.1098/rsta.2014.0166)
- Turner AK, Hunke EC, Bitz CM. 2013 Two modes of sea-ice gravity drainage: a parameterization for large-scale modeling. J. Geophys. Res. Ocean. 118, 2279–2294. (doi:10.1002/jgrc.20171)
- 24. Pringle DJ. Thermal conductivity of sea ice and antarctic permafrost. PhD thesis. Victoria University of Wellington, Wellington, New Zealand. https://seaice.alaska.edu/gi/publications/pringle/04Pringle\_PhD.pdf.
- 25. Bergman DJ. 1980 Exactly solvable microscopic geometries and rigorous bounds for the complex dielectric constant of a two-component composite material. *Phys. Rev. Lett.* 44, 1285–1287. (doi:10.1103/PhysRevLett.44.1285)
- Milton GW. 1980 Bounds on the complex dielectric constant of a composite material. Appl. Phys. Lett. 37, 300–302. (doi:10.1063/1.91895)
- 27. Golden K, Papanicolaou G. 1983 Bounds for effective parameters of heterogeneous media by analytic continuation. *Commun. Math. Phys.* **90**, 473–491. (doi:10.1007/BF01216179)
- 28. Milton G, Golden K. 1985 Thermal conduction in composites. In *Thermal conductivity 18* (eds T Ashworth, DR Smith), pp. 571–582. Boston, MA: Springer US. (doi:10.1007/978-1-4684-4916-7\_54)
- Milton GW. 2002 Theory of composites. Cambridge, UK: Cambridge University Press. (doi: 10.1017/CBO9780511613357)

- 30. Hashin Z, Shtrikman S. 1962 A variational approach to the theory of the elastic behaviour of polycrystals. *J. Mech. Phys. Solids* **10**, 343–352. (doi:10.1016/0022-5096(62)90005-4)
- 31. Luciano R, Sacco E. 1998 Variational methods for the homogenization of periodic heterogeneous media. Eur. J. Mech. A/Solid. 17, 599–617. (doi:10.1016/S0997-7538(99)80024-2)
- 32. Torquato S. 2013 Random heterogeneous materials: microstructure and macroscopic properties. vol. 16. Cham, Switzerland: Springer.
- Murphy NB, Hallman D, Cherkaev E, Xin J, Golden KM. 2024 Spectral measures and iterative bounds for effective diffusivity of steady and space-time periodic flows. arXiv. See https://arxiv.org/abs/2404.18754.
- 34. Murphy NB, Cherkaev E, Zhu J, Xin J, Golden KM. 2020 Spectral analysis and computation for homogenization of advection diffusion processes in steady flows. *J. Math. Phys.* **61**, 1. (doi:10.1063/1.5127457)
- 35. Murphy NB, Cherkaev E, Xin J, Zhu J, Golden KM. 2017 Spectral analysis and computation of effective diffusivities in space-time periodic incompressible flows. *Ann. Math. Sci. Appl.* **2**, 3–66. (doi:10.4310/AMSA.2017.v2.n1.a1)
- Fannjiang A, Papanicolaou G. 1997 Convection-enhanced diffusion for random flows. J. Stat. Phys. 88, 1033–1076. (doi:10.1007/BF02732425)
- 37. McLaughlin DW, Papanicolaou GC, Pironneau OR. 1985 Convection of microstructure and related problems. *SIAM J. Appl. Math.* **45**, 780–797. (doi:10.1137/0145046)
- 38. Pavliotis GA. 2002 Homogenization theory for advection-diffusion equations with mean flow. PhD thesis. Rensselaer Polytechnic Institute, Troy, New York.
- 39. Majda AJ, Kramer PR. 1999 Simplified models for turbulent diffusion: theory, numerical modelling, and physical phenomena. *Phys. Rep.* **314**, 237–574. (doi:10.1016/S0370-1573(98)00083-0)
- Papanicolaou G, Varadhan S. 1982 Boundary value problems with rapidly oscillating coefficients. In *Colloquia mathematica societatis János bolyai 27, random fields (Esztergom, Hungary 1979)*, pp. 835–873. Amsterdam, The Netherlands: North-Holland.
- Papanicolaou G, Pironeau O. 1981 On the asymptotic behavior of motions in random flows.
   In *Stochastic nonlinear systems in physics, chemistry, and biology* (eds L Arnold, R Lefever), pp. 36–41. Berlin, Germany: Springer. (doi:10.1007/978-3-642-68038-0\_4)
- 42. Taylor GI. 1922 Diffusion by continuous movements. *Proc. Lond. Math. Soc.* **2**, 196–212. (doi: 10.1112/plms/s2-20.1.196)
- 43. Bhattacharya RN, Gupta VK, Walker HF. 1989 Asymptotics of solute dispersion in periodic porous media. *SIAM J. Appl. Math.* 49, 86–98. (doi:10.1137/0149005)
- 44. Avellaneda M, Majda A. 1989 Stieltjes integral representation and effective diffusivity bounds for turbulent transport. *Phys. Rev. Lett.* **62**, 753–755. (doi:10.1103/PhysRevLett.62. 753)
- 45. Rapp BE. 2022 *Microfluidics: modeling, mechanics and mathematics*. Amsterdam, The Netherlands: Elsevier Science.
- 46. Baker GA, Graves-Morris PR. 1996 Padé approximants. In *Encyclopedia of mathematics and its applications*. Cambridge, UK: Cambridge University Press.
- 47. Bhattacharya R. 1999 Multiscale diffusion processes with periodic coefficients and an application to solute transport in porous media. *Ann. Appl. Probab.* **9**, 951–1020. (doi:10. 1214/aoap/1029962863)
- 48. Biferale L, Crisanti A, Vergassola M, Vulpiani A. 1995 Eddy diffusivities in scalar transport. *Phys. Fluid.* 7, 2725–2734. (doi:10.1063/1.868651)
- 49. Frankenstein G, Garner R. 1967 Equations for determining the brine volume of sea ice from −0.5° to −22.9°C. *J. Glaciol.* **6**, 943−944. (doi:10.1017/S0022143000020244)
- Golden KM, Eicken H, Heaton AL, Miner J, Pringle DJ, Zhu J. 2007 Thermal evolution of permeability and microstructure in sea ice. *Geophys. Res. Lett.* 34, 16. (doi:10.1029/ 2007GL030447)
- Freitag J, Eicken H. 2003 Meltwater circulation and permeability of Arctic summer sea ice derived from hydrological field experiments. *J. Glaciol.* 49, 349–358. (doi:10.3189/ 172756503781830601)
- Guéguen Y, Gavrilenko P, Le Ravalec M. 1996 Scales of rock permeability. Surv. Geophys. 17, 245–263. (doi:10.1007/BF01904043)

royalsocietypublishing.org/journal/rspa

- 53. Huysmans M, Dassargues A. 2005 Review of the use of Péclet numbers to determine the relative importance of advection and diffusion in low permeability environments. *Hydrogeol. J.* **13**, 895–904. (doi:10.1007/s10040-004-0387-4)
- De Ghislain M. 1986 Quantitative hydrogeology: groundwater hydrology for engineers. New York, NY: Academic Press.
- 55. Ahoulou AWA, Tinet A -J., Oltéan C, Golfier F. 2020 Experimental insights into the interplay between buoyancy, convection, and dissolution reaction. *J. Geophys. Res.* **125**, e2020JB020854. (doi:10.1029/2020JB020854)
- 56. Wells AJ, Hitchen JR, Parkinson JRG. 2019 Mushy-layer growth and convection, with application to sea ice. *Phil. Trans. R. Soc. A* 377, 20180165. (doi:10.1098/rsta.2018.0165)
- 57. Pavliotis GA. 2014 Stochastic processes and applications: diffusion processes, the Fokker-Planck and Langevin equations. vol. **60**. New York, NY: Springer. (doi:10.1007/978-1-4939-1323-7)
- 58. Cotter CJ, Pavliotis GA. 2009 Estimating eddy diffusivities from noisy Lagrangian observations. *Commun. Math. Sci.* 7, 805–838. (doi:10.4310/CMS.2009.v7.n4.a2)
- 59. Gardiner CW. 1985 *Handbook of stochastic methods: for physics, chemistry and the natural sciences*. Berlin, Germany: Springer-Verlag. (doi:10.1007/978-3-662-02452-2)
- 60. Evans L. 2013 *An introduction to stochastic differential equations*. Providence, RI: American Mathematical Society. (doi:10.1090/mbk/082)
- 61. Kloeden PE, Platen E. 2013 *Numerical solution of stochastic differential equations.* vol. 23. Berlin, Germany: Springer.
- 62. Pringle DJ, Trodahl HJ, Haskell TG. 2006 Direct measurement of sea ice thermal conductivity: no surface reduction. *J. Geophys. Res. Ocean.* **111**, C5. (doi:10.1029/2005]C002990)
- 63. Kwok R, Untersteiner N. 2011 The thinning of Arctic sea ice. *Phys. Today* **64**, 36–41. (doi:10. 1063/1.3580491)
- Kraitzman N. 2024 Enhanced thermal transport in sea ice. Zenodo. See https://doi.org/10. 5281/zenodo.10901754.